RESEARCH PAPER

Synthesis of Carbon Doped SnO_2 Quantum dots for Enhanced Visible-Light driven Photocatalytic degradation of Eosin Y

Dinesh Bourasi[1]*, Jayesh Bhatt[2], Seema Kothari[3]

[1,2,3]*Department of chemistry, Pacific Academy of Higher Education and Research University. Udaipur, 313003 (Rajasthan), INDIA*

Corresponding Author

Dinesh Bourasi

Research Scholar, Department of Chemistry, Pacific Academy of Higher Education and Research University, Udaipur-313003, Rajasthan, India, Email- dns165br@gmail.com

ABSTRACT

Discharge of synthetic organic dye pollutants continues to result in irreversible damage to aquatic environments due to the rapid industrialization, growing urbanization and extensive use of non-sustainable resources. In particular, carbon-doped SnO_2 quantum dots (C-doped SnO_2 QDs) are interesting due to their visible-light photocatalytic activity, which is achieved through their nanoscale particle size, large surface area and efficient charge separation. In the current work, carbon doped SnO_2 quantum dots were synthesized through simple hydrothermal technique with some modifications. The synthesized quantum dots were analyzed by X-ray diffraction (XRD), Field Emission Scanning Electron Microscopy (FESEM), Energy Dispersive Spectroscopy (EDS) and elemental mapping, High Resolution Transmission Electron Microscopy (HRTEM) with Selected Area Electron Diffraction (SAED), Fourier-transform Infrared Spectroscopy (FTIR), Diffuse Reflectance Spectroscopy (DRS) and X-ray Photoelectron Spectroscopy (XPS). The visible-light photocatalytic degradation of Eosin Y dye was investigated using a 200 W tungsten lamp. The apparent rate constant was systematically studied with respect to the pH, initial dye concentration, catalyst loading and light intensity. Dye concentration of 0.8×10^{-5} M, catalyst loading of 0.040 g, pH of 8.5, and light intensity of 70 $mWcm^{-2}$ were the optimum conditions which led to the maximum apparent rate constant of 3.76×10^{-4} s^{-1}. Pseudo-first order kinetic was obtained and confirmed by the linearity of (2 + log A) vs. time plots in degradation kinetics. The photocatalytic activity of carbon doped SnO_2 QDs was found to be significantly higher than that of undoped SnO_2 QDs under similar conditions due to the formation of a higher number of reactive oxidative species under visible light irradiation.

Keywords: Carbon-doped SnO_2; Quantum dots; Photocatalytic degradation; Eosin Y; Visible-light photocatalysis; Pseudo-first-order kinetics.

How to cite this article: Bourasi D, Bhatt J, Kothari S. Synthesis of Carbon Doped SnO_2 Quantum dots for Enhanced Visible-Light driven Photocatalytic degradation of Eosin Y. Int J Drug Deliv Technol. 2026;16(58s):1739-1752. DOI: 10.25258/ijddt.16.58s.186

1. INTRODUCTION

Persistent organic pollutants (POPs) are one of the most important aqueous pollutants generated by the massive industrial dyeing of textile, pharmaceutical, and food production.[1-2] Of these, xanthene dyes like Eosin Y (Figure 1) are of great interest because of their high chemical stability, resistance to biodegradation, and toxic effects such as carcinogenicity and persistence in the environment.[1] These compounds, even at low concentrations, can generate strong colours in receiving water bodies, reduce light penetration and impact aquatic ecosystems.[3] The removal or mineralization of these pollutants using conventional wastewater treatment technologies is often insufficient, such as adsorption, coagulation, and biological degradation.[4-5]This has led to the creation of advanced, effective and sustainable treatment strategies.[6-7]

Semiconductor-based heterogeneous photocatalysis has been one of the most promising technologies for wastewater treatment because it allows the generation of reactive oxygen species (ROS) by absorbing light for the degradation of organic contaminants in water.[8-10] Under the onset of light, photocatalytic processes driven by semiconductor materials create ROS and mediate the

decomposition of pollutants into less dangerous and/or complete mineralization.[11] Although more widely studied photocatalysts like TiO_2 and ZnO are chemically stable, inexpensive and highly oxidative, their practical application is limited due to their large bandgap, which results in the confinement of photoactivity to the ultraviolet region of the spectrum and fast recombination of the photogenerated electron–hole pairs.[12-13] Therefore, visible-light active semiconductor photocatalysts having high charge separation efficiency are still important research topics.

The chemical stability, non-toxicity and favourable oxidation potential of SnO_2 have spurred increasing interest in the use of SnO_2 as an alternative photocatalyst.[14-16] However, SnO_2 has a relatively large band gap (~3.6 eV) and poor charge separation, restricting its use for photocatalytic applications in the visible light range of the spectrum.[8,16,17] To tackle these challenges, nanostructuring and doping with heteroatoms have been suggested as promising approaches [12,18]. The quantum confinement effect brings unique benefits to quantum dots such as tunable band gaps, heightened surface reactivity, and improved charge transport properties.[19-21] Specifically, carbon and nitrogen doping has been proven to shift the absorption peak towards the visible range and reduce the recombination of electron–hole pairs.[22-24] These properties of carbon incorporation can create mid-gap energy states, increase charge-carrier mobility and enable interfacial electron transfer in semiconductor systems.[25-27] Although these achievements have been accomplished, the studies examining the photocatalytic degradation of xanthene dyes under visible light illumination with carbon doped SnO_2 quantum dots are still rather limited in terms of systematic optimization of the operational parameters and commenting on the mechanism.

In the present study, carbon doped SnO_2 quantum dots were synthesized by modifying the hydrothermal method and the photocatalytic degradation of eosin Y dye was investigated under visible-light irradiation. The degradation efficiency and apparent rate constants are systematically studied as a function of the key operating conditions such as solution pH, initial dye concentration, catalyst loading and light intensity. Kinetics of degradation are studied and a mechanism is suggested from experiment. The results will help to develop effective photocatalysts that can be activated by visible light for sustainable water treatment.

2. MATERIALS AND METHOD

2.1 Synthesis of C-Doped and Pure SnO_2 Quantum Dots

Carbon-doped and undoped SnO_2 quantum dots were synthesized following a modified methodology reported by Tirado-Guízar et al.[28] A solution containing 4 mmol of $SnCl_4 \cdot 5H_2O$ in 20 mL of deionized water was mixed with a solution containing 2 mmol of glucose in 20 mL of deionized water and stirred for 10 min. A solution containing 40 mmol of urea in 30 mL of deionized water was then gradually added under continuous stirring. The final mixture was transferred to a Teflon-lined autoclave and maintained at 90°C for 5 h, after which it was allowed to cool to room temperature. The precipitate was collected by centrifugation, washed five times with deionized water and twice with absolute ethanol, and dried in an oven at 60°C overnight. The dried material was subsequently calcined in a muffle furnace at 400 °C for 2 h to yield carbon-doped SnO_2 quantum dots. Pure (undoped) SnO_2 quantum dots were prepared by an identical procedure, substituting 20 mL of deionized water for the glucose solution to maintain the same total liquid volume.

2.2 Characterization

X-ray diffraction (XRD) patterns were recorded on a PANalytical, Netherlands, X'Pert Pro diffractometer using Cu Kα radiation (λ = 0.15406 nm). FESEM images and EDS/elemental mapping were acquired on a SU-8010 Series instrument (Hitachi, Japan). HRTEM images and SAED patterns were recorded on a JEOL, JEM-2100 Plus. XPS measurements were performed on a Thermo Fisher Scientific, K-ALPHA system. FTIR spectra were recorded on a Bruker ALPHA II spectrometer. UV-Vis diffuse reflectance spectra (DRS) were recorded on a PerkinElmer, USA, Lambda19 UV-VIS-NIR Spectrophotometer.

2.3 Photocatalytic Activity

The photocatalytic activity of the catalyst was assessed by monitoring the degradation of Eosin Y dye (λmax = 517 nm). A stock solution of 1.0×10^{-3} M was prepared by dissolving the appropriate mass of Eosin Y in 100 mL of doubly distilled water; working solutions of the required concentration were prepared from this stock. Solution pH was adjusted using 0.1 N HCl and 0.1 N NaOH solutions. Irradiation was carried out using a 200 W tungsten lamp; light intensity was varied by adjusting the distance between the lamp and the reaction vessel. Aliquots were withdrawn at regular time intervals, and the absorbance was measured at 517 nm using a UV-Vis spectrophotometer. A plot of (2 + log A) against irradiation time was found to be linear for both C-doped SnO_2 QDs and pure SnO_2 QDs, confirming pseudo-first-order degradation kinetics. The apparent rate constant was determined from:

$k = 2.303 \times Slope$

The molecular structure of Eosin Y dye used in the study is shown in Figure 1.

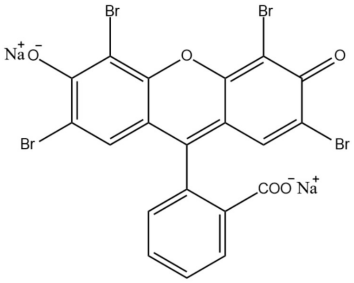

Figure 1. Structure of Eosin Y

3.RESULTS AND DISCUSSION

3.1 X-Ray Diffraction (XRD)

The crystalline structure of the synthesized C-doped SnO_2 quantum dots was examined by XRD (PANalytical X'Pert Pro, Cu Kα radiation, λ = 0.15406 nm). The XRD pattern in Fig. 2 displays diffraction peaks corresponding to the tetragonal rutile-type SnO_2 with a cassiterite structure, consistent with JCPDS card No. 41-1445. A slight shift in peak positions compared to standard bulk SnO_2 was observed, suggesting lattice distortion induced by carbon incorporation.[17,29] No diffraction peaks attributable to carbon or other impurity phases were detected, confirming phase purity. The average crystallite size was estimated using the Debye–Scherrer equation:

$$D = K\lambda / (\beta \cos \theta)$$

where D is the mean crystallite size, K = 0.9 is the dimensionless shape factor, λ = 0.15406 nm is the X-ray wavelength (Cu Kα), β is the full-width at half-maximum (FWHM) of the diffraction peak in radians, and θ is the Bragg's angle. Using the most intense diffraction peak at the (110) plane, the calculated crystallite size was approximately 3.2 nm, confirming the quantum dot nature of the synthesized material.[24]

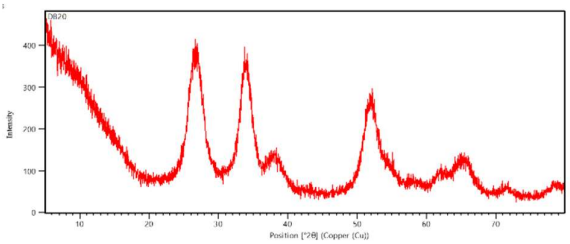

Figure 2. XRD pattern of carbon-doped SnO_2 quantum dots showing characteristic peaks of the rutile phase.

3.2 Field Emission Scanning Electron Microscopy (FESEM)

FESEM images of C-doped SnO_2 QDs recorded on Hitachi, SU-8010 Series are presented in Figure 3. The images reveal agglomerated crystalline nanoparticles with a wheat-grain-like morphology, characteristic of hydrothermally synthesized SnO_2 nanomaterials.[30]

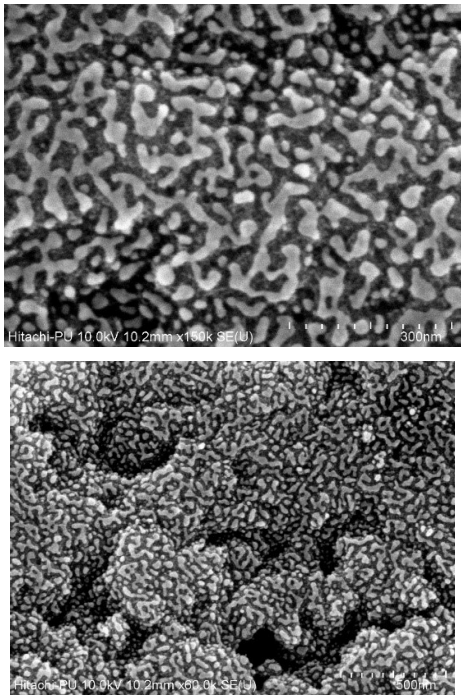

Figure 3. FESEM images of carbon-doped SnO_2 quantum dots showing agglomerated nanostructures

3.3 Energy Dispersive Spectroscopy (EDS) and Elemental Mapping

The elemental composition was determined by EDS (integrated with FESEM, Hitachi, SU-8010 Series) shown in Fig. 4. The EDS spectrum confirmed the presence of Sn (30.02 at.%), O (62.22 at.%), and C (7.76 at.%) as the sole constituent elements, with no additional elemental impurities, establishing successful carbon incorporation into the SnO_2 nanostructure. Elemental mapping in Fig.5 demonstrates uniform spatial distribution of Sn, O and C across the sample matrix, confirming homogeneous carbon doping.[24,31]

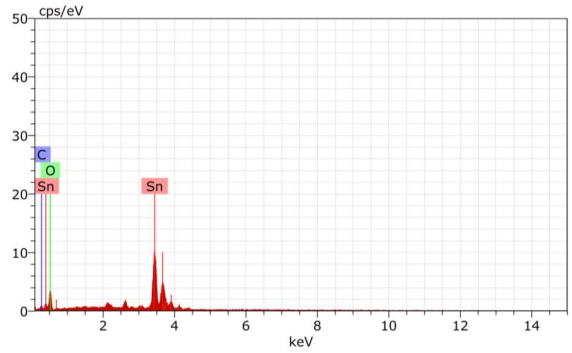

Figure 4. EDS spectrum of carbon-doped SnO_2 quantum dots confirming elemental composition.

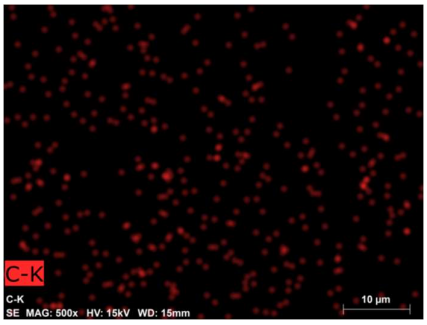

Figure 5. Images of elemental mapping with uniform distributions of Sn, O and C.

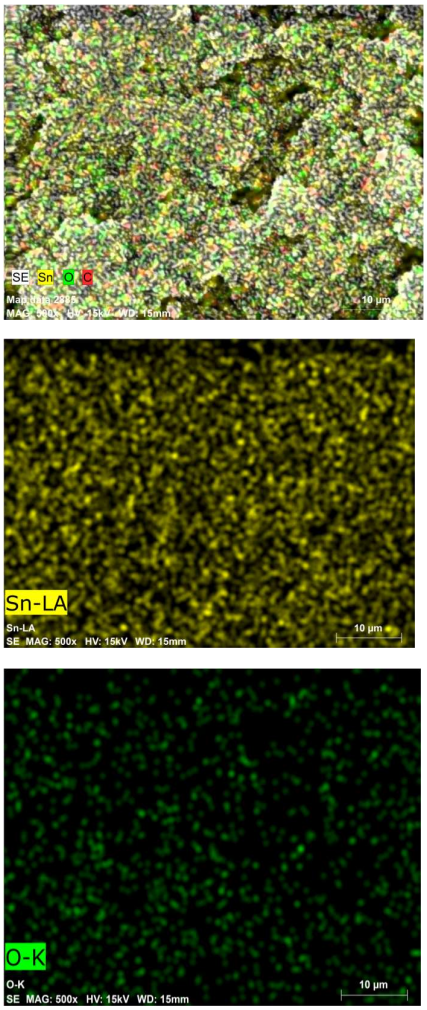

3.4 HRTEM and SAED Analysis

HRTEM analysis by JEOL, JEM-2100 Plus, indicates SnO_2 quantum dots exhibiting quasi-spherical shape uniformly distributed with particle size between 2.5-6nm (Fig.6(a-b)). The average diameter from particle size distribution (PSD) has been determined by the ImageJ software and is around 3.4 nm, which is presented as histogram in Fig 6 (c). This is similar to the results obtained from XRD. This is an indication of quantum dot nature of the synthesized material (with particle size < 10nm).[19,33] SAED pattern in Fig.6(d) revealed concentric diffraction rings corresponding to (110), (101), (211) and (301) planes of tetragonal rutile SnO_2, which was indicative of polycrystalline nature with broadening characteristics of the ultrafine nanocrystals.[16,32]

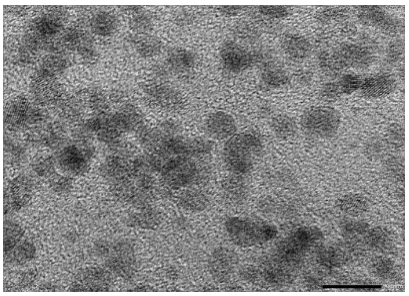

(a)

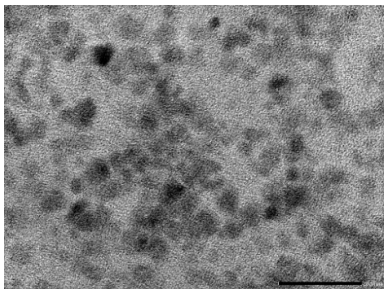

(b)

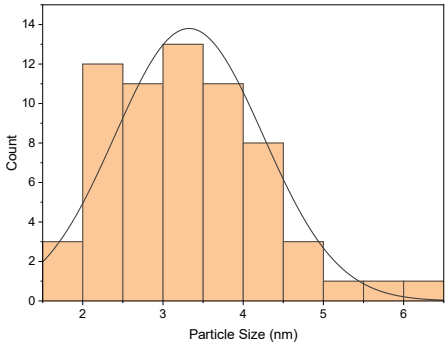

(c)

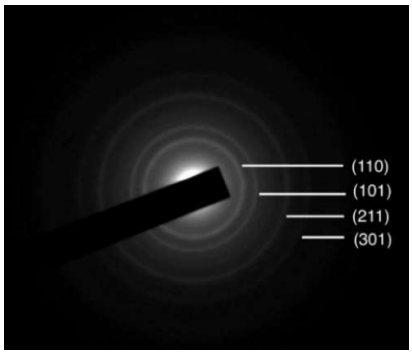

(d)

Figure 6. (a–b) HRTEM images, (c) particle size distribution (d) SAED pattern

3.5 FT-IR Spectroscopy

FTIR spectra were recorded by Bruker ALPHA II for the C-doped SnO_2 QDs is given in fig. 7. The broad band at ~3393 cm^{-1} is due to the –OH groups engaged in hydrogen bonding, while the band at ~1630 cm^{-1} is the bending vibration of the water molecules adsorbed on the surface.[31] The main features observed at 700–300 cm^{-1} are due to the crystal SnO_2 where the broadening is attributed to the nanocrystalline effect.[32] The band is located at ~600 cm^{-1} is attributed to the Sn–O–Sn fundamental stretching mode of the surface-bridging oxide, while the band at ~530 cm^{-1} is assigned to the vibration of terminal Sn–O bond of the Sn–OH groups.[31] A band appearing around 1040 cm^{-1} is related to metal oxides which have more than one oxygen atom attached to a single metal centre.

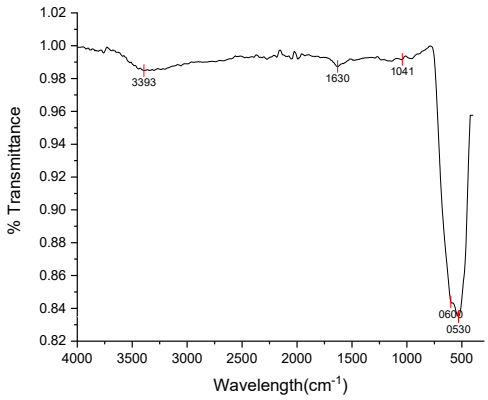

Figure 7. FTIR spectrum SnO_2 quantum dots after carbon doping with typical vibrational bands.

3.6 Optical Properties (Band Gap Analysis)

The optical properties of the synthesized photocatalysts were investigated using UV–Vis diffuse reflectance spectroscopy. The pure and C-doped SnO_2 QDs were characterized by recording their DRS on PerkinElmer Lambda19 UV-VIS-NIR Spectrophotometer. The optical band gap energies were obtained by using the Kubelka–Munk function, F(R∞), which is given by:

$$F(R_\infty) = (1 - R_\infty)^2 / (2R_\infty) = K / S$$

where R_∞ is the reflectance of an infinitely thick sample, and K is the absorption coefficient and S is the scattering coefficient. Since the semiconductor possesses a direct electronic transitions, the linear extrapolation of $[F(R_\infty)\cdot h\nu]^2$ to the x-axis in the Tauc plot of $[F(R_\infty)\cdot h\nu]^2$ vs. photon energy hν (eV) was used to estimate the optical bandgap. Bands gap of the C-doped SnO_2 QDs was found to be 3.3 eV compared to the pure SnO_2 QDs where it was found to be 3.7 eV, which was presented in inset Tauc plot in Fig 8(a) and Fig 8(b) respectively.

The size of the crystallites in pure QDs is comparable to the Bohr radius, so it is expected that the bandgap energy will increase, due to quantum confinement effect.[33-34] In the present investigation, it was found that the bandgap of SnO_2 QDs got reduced with the increase in the annealing temperature and further reduced in C-doped SnO_2 QDs.[35] This is the reason for the improved ability of C-doped SnO_2 QDs to absorb and photocatalyze in visible light as compared to pure SnO_2 QDs.

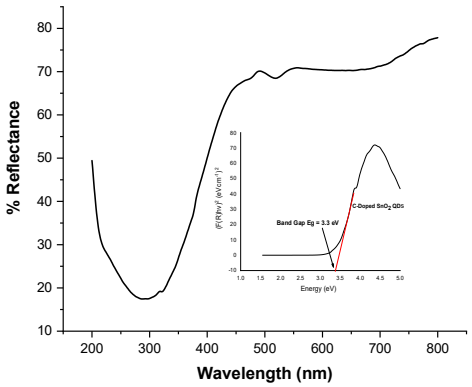

(a)

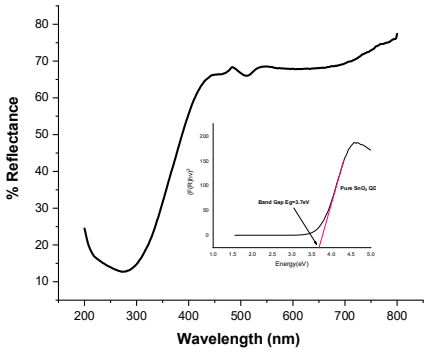

(b)

Figure 8. (a) DRS of C-doped SnO_2 QDs (b) Pure SnO_2 QDs together with the inset Tauc plot

3.7 XPS Analysis

To find the oxidation states and elemental composition, the C-doped SnO_2 QDs were characterized by XPS, Thermo Fisher Scientific, K-ALPHA (Fig 9(a-d)). The wide survey spectrum confirms the presence of Sn, O and C. The Sn 3d core level spectrum shows two peaks at 487.2 eV and 495.6 eV corresponding to Sn $3d_{5/2}$ and Sn $3d_{3/2}$ levels, respectively, which indicates the oxidation state of Sn^{4+}.[31,32] The single symmetric Sn $3d_{5/2}$ component indicates that there are no Sn^{2+} ions present. The O 1s peak at 531.35 eV is found to be in accordance with lattice oxygen of SnO_2.[16] The C 1s spectrum shows a peak at 285.35 eV, which is related to the incorporation of carbon.[24]

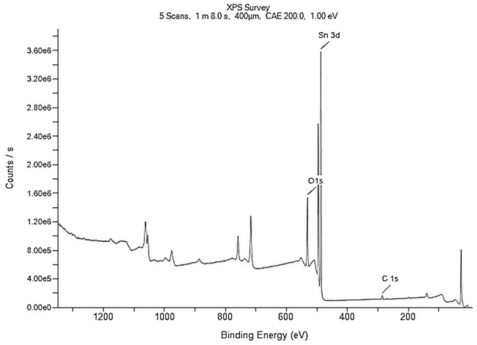

(a)

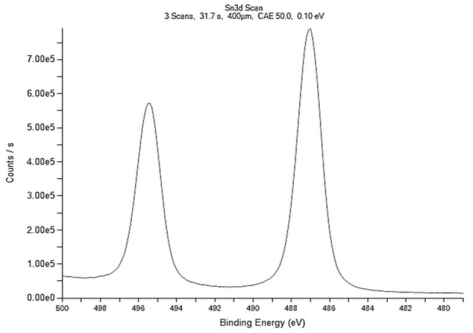

(b)

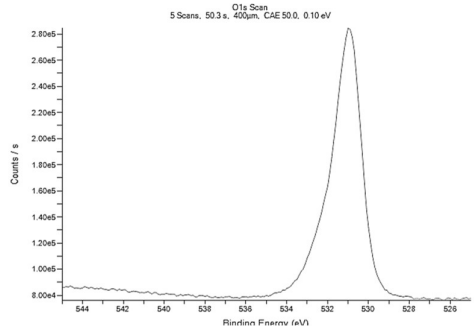

(c)

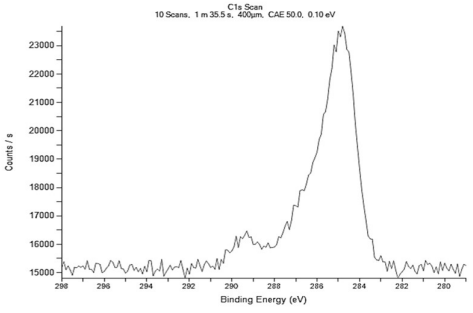

(d)

Fig. 9. XPS spectra of (a) survey (b) Sn 3d (c) O1s and (d) C 1s of C-doped SnO_2 QDs.

3.8 Photocatalytic Degradation of Eosin Y

C-doped SnO_2 QDs were evaluated by monitoring the degradation of Eosin Y (517 nm) under visible-light irradiation. Both C-doped and pure SnO_2 QDs showed a decrease in absorbance as more time irradiated. The linear plots obtained for both catalysts suggest that the photocatalytic degradation of Eosin Y is pseudo-first-order reaction. The rate constant was calculated using the plot of k = 2.303 × Slope. The linearity of the plots indicates that photocatalytic degradation mostly occurs through surface-mediated oxidative reactions typical of heterogeneous photocatalytic systems.[8,36]

3.9 A Typical Run: Comparative Study of C-Doped and Pure SnO_2 QDs

A typical run was conducted at the following fully optimized conditions (dye concentration = 0.8×10^{-5} M, pH = 8.5, catalyst loading = 0.040 g, light intensity = 70 $mWcm^{-2}$, λ = 517 nm). Two studies were carried out, one for the C-doped SnO_2 QDs and another for the pure SnO_2 QDs. The results are presented in Table 1 and shown in Figure 10. The values of (2 + log A) decreased more rapidly with the irradiation time for the C-doped SnO_2 QDs than for the pure SnO_2 QDs, thus yielding a considerably higher apparent rate constant for the C-doped SnO_2 QDs (3.76×10^{-4} s^{-1}) than for the pure SnO_2 QDs (2.65×10^{-4} s^{-1}). The increased photocatalytic activity is due to the reduced optical band gap of the C-doped SnO_2 QDs (3.3 eV compared to 3.7 eV for pure SnO_2 QDs), which facilitates the absorption of more photons in the visible region resulting in a greater number of reactive oxidative species. These results show that the visible-light photocatalytic activity of SnO_2 QDs is greatly enhanced by the incorporation of carbon.

Table 1. A Typical Run: Comparative Photocatalytic Degradation of Eosin Y Using C-Doped and Pure SnO_2 Quantum Dots

Experimental conditions: Dye concentration = 0.8×10^{-5} M; catalyst loading = 0.040 g; light intensity = 70 mW cm^{-2}; pH = 8.5; λ = 517 nm

Time (min)	C-Doped SnO_2 QD Absorbance (A)	C-Doped SnO_2 QDs 2 + log A	Pure SnO_2 QD Absorbance (A)	Pure SnO_2 QDs 2 + log A
0	0.63	1.7993	0.63	1.7993
15	0.485	1.6857	0.565	1.752
30	0.39	1.5911	0.487	1.6875
45	0.253	1.4031	0.399	1.601
60	0.179	1.2529	0.3	1.4771
75	0.116	1.0645	0.227	1.356
90	0.097	0.9868	0.158	1.1987
105	0.061	0.7853	0.141	1.1492
120	0.045	0.6532	0.115	1.0607

Rate constant: C-doped SnO_2 QDs = 3.76×10^{-4} s^{-1}; Pure SnO_2 QDs = 2.65×10^{-4} s^{-1}

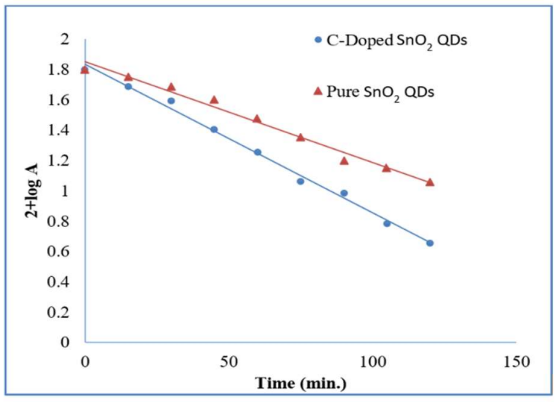

Rate constant: C-doped SnO_2 QDs = 3.76×10^{-4} s^{-1}
Pure SnO_2 QDs = 2.65×10^{-4} s^{-1}.

Figure 10. A Typical Run Showing Comparative Degradation of Eosin Y by C-Doped and Pure SnO_2 QDs (2 + log A vs. Time)

3.10 Effect of pH

The effect of pH on the rate of photocatalytic degradation of Eosin Y was investigated over the range pH 6.0 to 9.5. The results are presented in tabular form (Table 2) and as a graph (Figure 11). The degradation rate was found to be progressively higher in the range of pH 6.0 to a maximum at pH 8.5 (k = 3.76 x 10^{-4} s^{-1}) and then decreased at higher pH values. The increase in degradation rate with pH is believed to be due to the greater production of hydroxyl radicals (•OH) from the OH^- ions available, which are more abundant under alkaline conditions. Moreover, at higher pH values, Eosin Y continuously deprotonates to produce ionic species which can better interact with the catalyst surface. Outside of this range, higher charge recombination and competitive scavenging effect decreases the effective concentration of ROS, leading to a decrease in degradation rate.

Table 2. Effect of pH on Photocatalytic Degradation of Eosin Y

pH	Rate Constant,

	$k \times 10^4$ (s^{-1})
6	2.3
6.5	2.22
7	2.26
7.5	2.75
8	3.26
8.5	3.76
9	3.26
9.5	3.23

Experimental conditions: Dye concentration = 0.8×10^{-5} M; catalyst loading = 0.040g; light intensity = 70 $mWcm^{-2}$; λ = 517 nm.

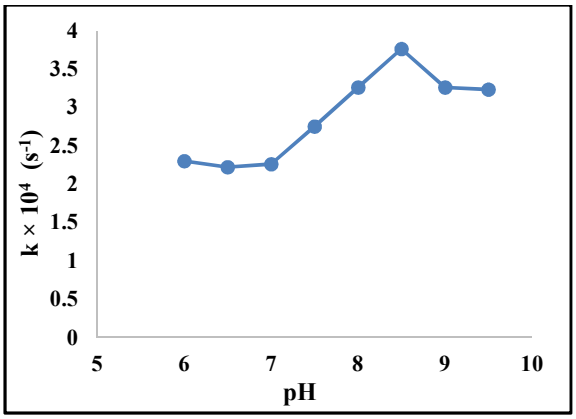

Figure 11. Effect of pH

3.11 Effect of Eosin Y Concentration

The initial concentration of Eosin Y was varied between 0.6×10^{-5} and 2.0×10^{-5} M and its effect on degradation rate was investigated. Summary of the results is given in Table 3 and graphically in Figure 12. The rate constant was seen to rise with the increasing concentration of dye up to a maximum concentration of 0.8×10^{-5} M ($k = 3.76 \times 10^{-4}$ s^{-1}), after which it went on decreasing. The first enhancement in the degradation rate is attributed to the increased availability of Eosin Y molecules for excitation and energy/electron transfer to the surface of the catalyst. When the refractive index of the dye exceeds 0.8×10^{-5} M, the dye will serve as an inner filter, blocking the incoming visible light, and decreasing the number of photons that reach the surface of the catalyst. Moreover, at higher concentration, the unbound dye molecules will compete for the active catalytic surface sites in the presence of which less dye molecules will be available for interaction with the reactive species generated by the semiconductor, thereby showing a decrease in the rate constant.[11,13]

Table 3. Effect of Eosin Y Concentration on Photocatalytic Degradation

[Eosin Y] $\times 10^5$ M	Rate Constant, $k \times 10^4$ (s^{-1})
0.6	2.56
0.8	3.76
1	2.05
1.2	1.2
1.4	0.94
1.6	1.02
1.8	0.94
2	0.77

Experimental conditions: pH = 8.5; catalyst loading = 0.040 g; light intensity = 70 $mWcm^{-2}$; λ = 517 nm.

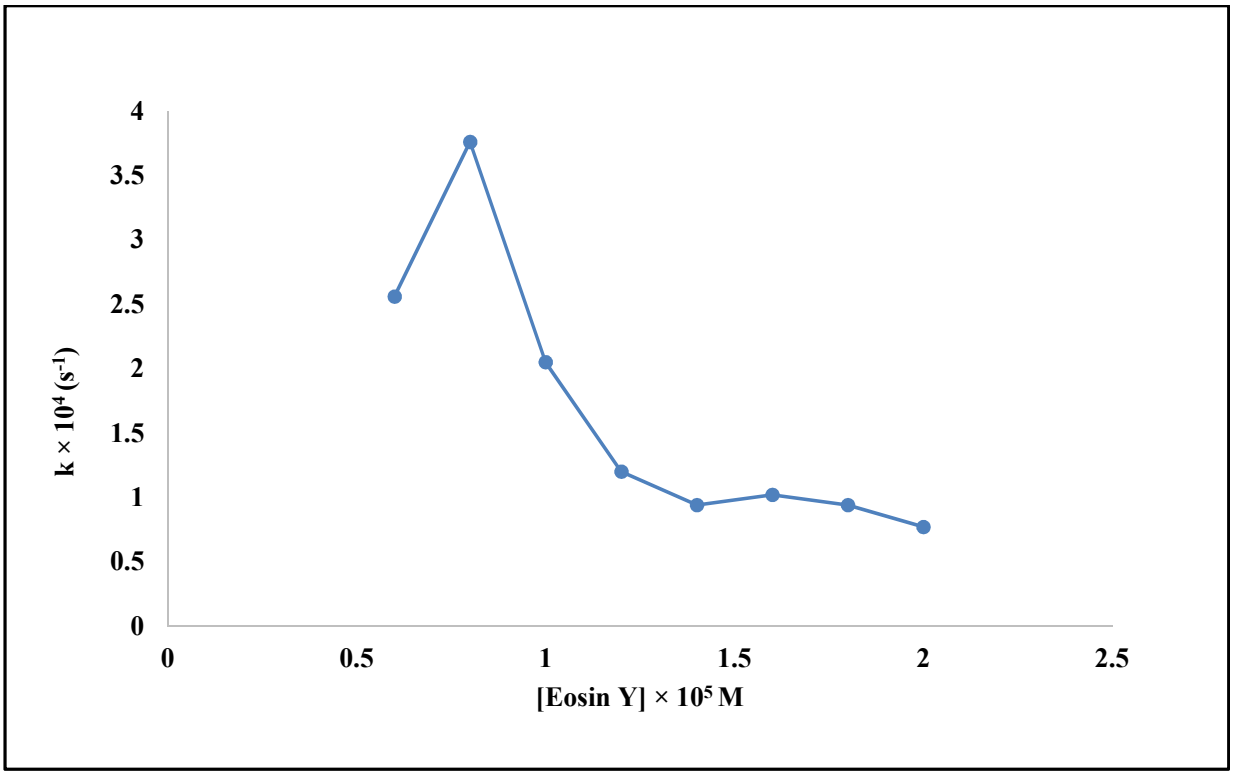

Figure 12. Effect of Eosin Y Concentration

3.12 Effect of Amount of C-doped SnO_2 QDs

The effect of the amount of C-doped SnO_2 QDs on the rate of Eosin Y degradation was investigated over the range 0.02–0.14 g. The results are summarized in Table 4 and presented graphically in Figure 13. The apparent rate constant rose with the loading of the catalyst till optimum value 0.040 g ($k = 3.76 \times 10^{-4}$ s^{-1}) and then began to fall. The first increase of degradation rate is due to the increased number of surface sites that are available for the absorption of photons and formation of ROS. For loadings larger than 0.040 g, the higher concentration of the catalyst leads to greater aggregation and light scattering and thus lower photon penetration and lower apparent rate constant.

Table 4. Effect of amount of C-doped SnO_2 QDs on Photocatalytic Degradation of Eosin Y

C-doped SnO_2 QDs (g)	Rate Constant, $k \times 10^4$ (s^{-1})
0.02	2.14
0.04	3.76
0.06	2.31
0.08	1.54
0.1	1.02
0.12	0.94
0.14	1.03

Experimental conditions: pH = 8.5; dye concentration = 0.8×10^{-5} M; light intensity = 70 $mWcm^{-2}$; λ = 517 nm.

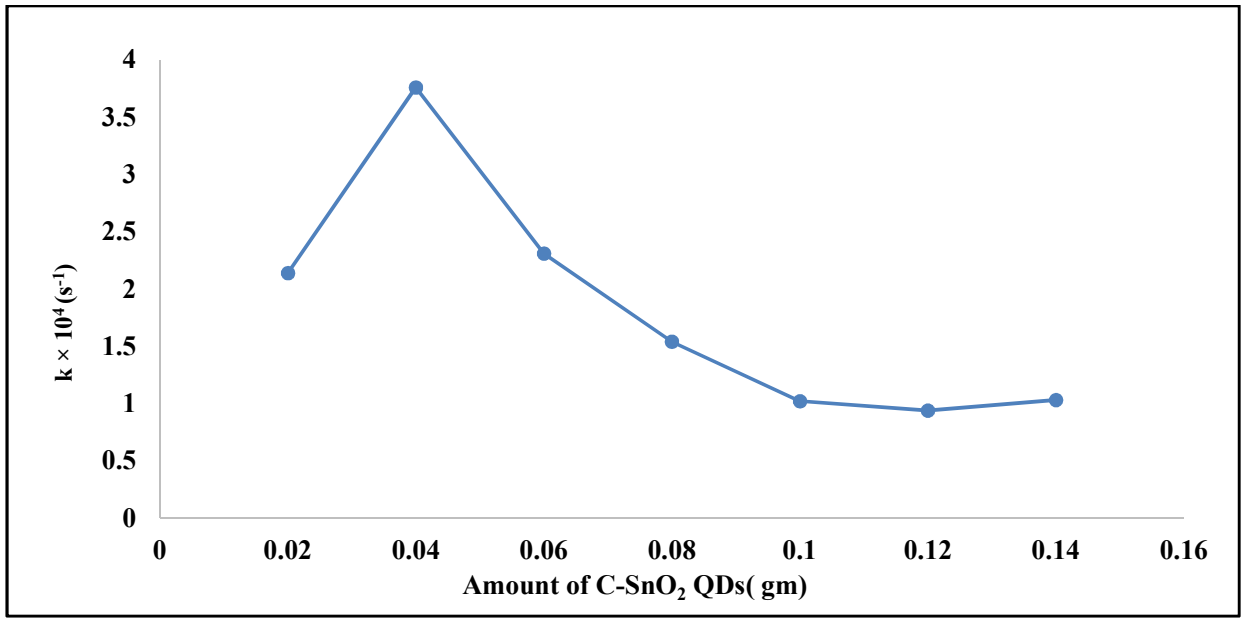

Figure13. Effect of amount of C-doped SnO_2 QDs

3.13 Effect of Light Intensity

The effect of visible-light intensity on the rate of degradation of Eosin Y was examined by changing the distance between the 200 W tungsten lamp and the reaction vessel (20–70 $mWcm^{-2}$). Results are summarised in Table 5 and graphically presented in Figure 14. The apparent rate constant showed a increase with the intensity of the light reaching a maximum value of 3.76×10^{-4} s^{-1} at 70 $mWcm^{-2}$. The degradation rate increased monotonously with light intensity as shown in the range studied, due to the higher photon flux that falls on the surface of the catalyst leading to the higher generation of electron–hole pairs, and consequently, the higher concentration of reactive oxygen species such as hydroxyl radicals (•OH) and superoxide radical anions ($•O_2^-$).[8,9] As the photon flux increased, the rate increment was also observed to increase, implying that it was the photon flux that is the limiting factor under the experimental conditions studied.

Table 5. Effect of Light Intensity on Rate of Photocatalytic Degradation of Eosin Y

Light Intensity ($mWcm^{-2}$)	Rate Constant, $k \times 10^4$ (s^{-1})
20	0.83
30	0.98
40	1.37
50	2.66
60	3.6
70	3.76

Experimental conditions: pH = 8.5; dye concentration = 0.8×10^{-5} M; catalyst loading = 0.040 g; λ = 517 nm.

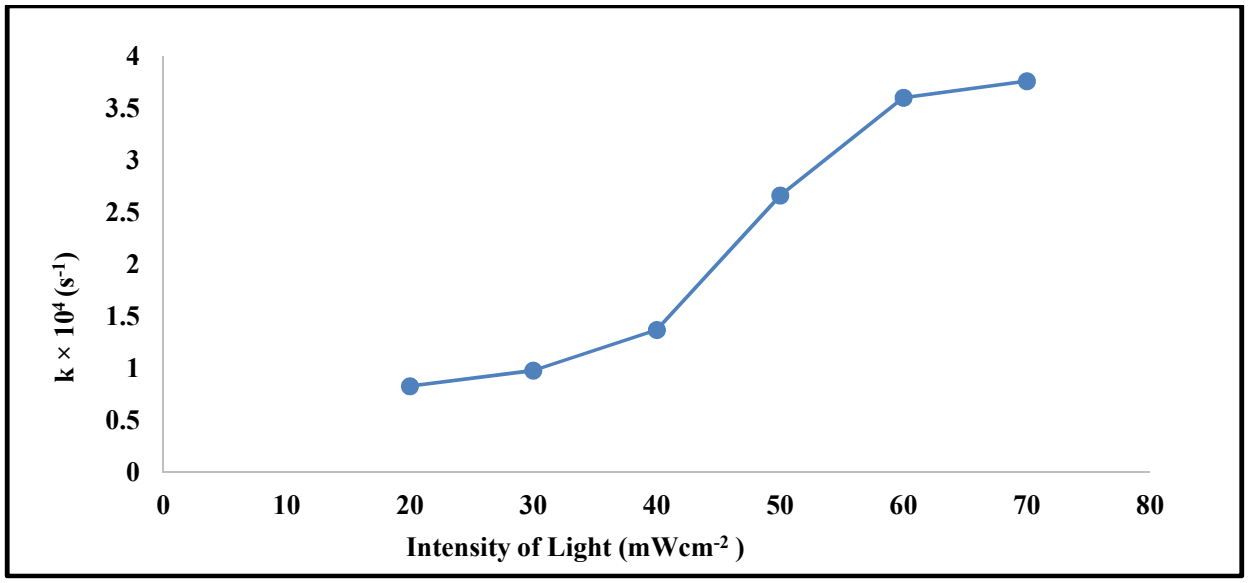

Figure 14. Effect of Light Intensity

3.14 Mechanism

With the above experimental findings, a tentative mechanism is proposed for photocatalytic degradation of Eosin Y by the C-doped SnO_2 QDs that is depicted in Figure 15. The appropriate visible light was absorbed by Eosin Y and excited to the first singlet excited state, which then intersystem crossing (ISC) to the triplet excited state. At the same time, the photons were absorbed by the C-doped SnO_2 QDs, and the electrons jumped from the valence band into the conduction band, forming electron–hole pairs. The photogenerated holes are able to withdraw electrons from hydroxyl ions (OH^-) or from adsorbed water to form hydroxyl radicals (•OH), and the photogenerated electrons react with dissolved oxygen to form superoxide radical anions ($•O_2^-$).[8,36] These ROS then oxidize Eosin Y molecules, triggering continual oxidation and mineralization to CO_2, H_2O and inorganic ions.

The primary oxidizing species in the reaction was found to be OH radicals on the basis of the use of the hydroxyl radical scavenger isopropyl alcohol (IPA), which resulted in significantly decreased degradation rate. It was also found that potassium iodide (KI) also slowed the degradation rate, suggesting that both hydroxyl radicals and photogenerated holes were responsible for the photocatalytic process. This is due to the narrower band gap of C doped SnO_2 QD (3.3 eV) than the pure SnO_2 QD (3.7 eV), higher absorption of visible light and more efficient charge carrier separation, which is more photocatalytic than pure SnO_2 QD.

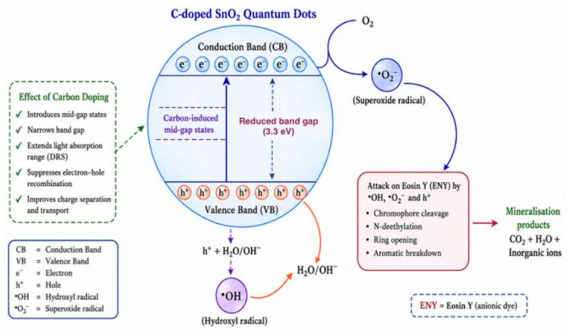

Figure 15. Proposed visible-light photocatalytic degradation mechanism of Eosin Y using C-doped SnO_2 quantum dots

C-doped SnO_2 QDs generate electron–hole pairs upon visible-light irradiation, generating ROS and subsequently undergoing oxidative degradation of Eosin Y.

CONCLUSION

The carbon doped SnO_2 quantum dots were successfully synthesized by modified hydrothermal method and systematically characterized by XRD, FESEM, EDS, HRTEM, FTIR, DRS and XPS analysis. Structural and spectroscopic studies proved that the phase-pure tetragonal SnO_2 quantum dots with carbon incorporation in semiconductor matrix were successfully prepared. The decreased optical bandgap from 3.7 eV to 3.3 eV from pure SnO_2 QDs to C-doped SnO_2 QDs was a proof of successful electronic structure modifications by incorporation of carbon and visible-light absorption properties.

Degradation of Eosin Y dye was used as a model reaction to assess the photocatalytic activity of the prepared C-doped SnO_2 QDs under visible-light conditions. The degradation kinetics were pseudo first order, and the effects of various operating parameters on the degradation process (pH, dye concentration, loading of catalyst and light intensity) were systematically studied. The optimum degradation conditions were found at a pH of 8.5, a dye concentration of 0.8×10^{-5} M, a catalyst amount of 0.040 g and a light intensity of 70 $mWcm^{-2}$, where the rate constant was 3.76×10^{-4} s^{-1}. Comparative studies showed that SnO_2 QDs doped with carbon had much greater photocatalytic efficiency than pure SnO_2 QDs, due to the greater efficiency in the utilization of visible light and the better charge-carrier separation.

The improved photocatalytic activity was attributed from the experimental results and scavenger studies to the increased production of ROS (hydroxyl radicals and superoxide radical anions) in the solution which increased the rate of degradation and mineralization of the molecules of the Eosin Y dye. The results suggest that SnO_2 quantum dots with carbon doping exhibit greatly enhanced photocatalytic properties in the visible light range and have a great potential for application in wastewater treatment with dye contaminants.

ACKNOWLEDGEMENT

The authors are thankful to SAIF/CIL, Panjab University, Chandigarh for XRD, FESEM, EDS, HRTEM, and XPS analyses; to SICART, Anand for diffuse reflectance spectroscopy, and to IIT Indore for FT-IR analysis. Sincere thanks are also extended to Pacific Academy of Higher Education and Research (PAHER) University for providing the necessary technical and experimental support.

REFERENCES

1. Mandal A, Kumar PS, Poorva CS, Raju LS, Balasubramani SR, Rangasamy G. Research progress of persistent organic pollutants in water: Classification, sources, potential risks, and treatment approaches. Water Pract Technol. 2024;19(3):937-959. https://doi.org/10.2166/wpt.2024.031
2. Rad SM, Ray AK, Barghi S. Water pollution and agriculture pesticide. Clean Technol. 2022;4(4):1088–1102. https://doi.org/10.3390/cleantechnol4040066
3. Wang R, Tang H, Yang R, Zhang J. Emerging contaminants in water environments: Progress, evolution, and prospects. Water Sci Technol. 2024;89(10):2763–2782. https://doi.org/10.2166/wst.2024.151
4. Khader EH, Mohammed TJ, Mirghaffari N, et al. Removal of organic pollutants from produced water by batch adsorption treatment. Clean Techn Environ Policy. 2022;24(3):713–720. https://doi.org/10.1007/s10098-021-02159-z
5. Knap-Bałdyga A, Żubrowska-Sudoł M. Natural organic matter removal in surface water treatment via coagulation—current issues, potential solutions, and new findings. Sustainability. 2023;15(18):13853. https://doi.org/10.3390/su151813853
6. Kaswan V, Kaur H. A comparative study of advanced oxidation processes for wastewater treatment. Water Pract Technol. 2023;18(5):1233–54. https://doi.org/10.2166/wpt.2023.061
7. Pérez H, Quintero García OJ, Amezcua-Allieri MA, Rodríguez Vázquez R. Nanotechnology as an efficient and effective alternative for wastewater treatment: An overview. Water Sci Technol. 2023;87(12):2971–3001. https://doi.org/10.2166/wst.2023.179
8. Wang H, Li X, Zhao X, Li C, Song X, Zhang P, Huo P. A review on heterogeneous photocatalysis for environmental remediation: from semiconductors to modification strategies. Chin J Catal. 2022;43(2):178–214. https://doi.org/10.1016/S1872-2067(21)63910-4
9. Balapure A, Ray Dutta J, Ganesan R. Recent advances in semiconductor heterojunctions: Fundamentals of photocatalysis, charge transfer mechanisms and materials. RSC Appl Interfaces. 2024;1(1):43–69. https://doi.org/10.1039/D3LF00126A
10. Buchude V, Kothari S. Photocatalytic Degradation of Eosin Yellow Dye using Ternary Nanocomposite g-C_3N_4/ZnO/CdS: A Sustainable solution for Water Pollution, Res. J. Chem. and Environ. 2026;30(4):145-149. https://doi.org/10.25303/304rjce1450149
11. Priyadarshini M, Das I, Ghangrekar MM, Blaney L. Advanced oxidation processes: Performance, advantages, and scale-up of emerging technologies. J Environ Manag. 2022;316(1):115295. https://doi.org/10.1016/j.jenvman.2022.115295
12. Rashid R, Shafiq I, Gilani MR, Maaz M, Akhter P, Hussain M, Jeong KE, Kwon EE, Bae S, Park YK. Advancements in TiO_2-based photocatalysis for environmental remediation: Strategies for enhancing visible-light-driven activity. Chemosphere. 2024;349(1):140703. https://doi.org/10.1016/j.chemosphere.2023.140703
13. Ong CB, Ng LY, Mohammad AW. A review of ZnO nanoparticles as solar photocatalysts: Synthesis, mechanisms and applications. Renew Sustain Energy Rev. 2018;81(1):536–551. https://doi.org/10.1016/j.rser.2017.08.020

14. Munawar T, Nadeem MS, Mukhtar F, Rehman MN, Riaz M, Batool S, Hasan M, Iqbal F. Transition metal-doped SnO_2 and graphene oxide (GO) supported nanocomposites as efficient photocatalysts and antibacterial agents. Environ Sci Pollut Res. 2022;29(60):90995–91016. https://doi.org/10.1007/s11356-022-22144-3

15. Vattikuti SVP, Sudhani HPK, Habila MA, Rosaiah P, Shim J. SnO_2 quantum dot-decorated g-C_3N_4 ultrathin nanosheets: A dual-function photocatalyst for pollutant degradation and hydrogen evolution. Catalysts. 2024;14(11):824. https://doi.org/10.3390/catal14110824

16. Bathula B, Gurugubelli TR, Yoo J, Yoo K. Recent progress in the use of SnO_2 quantum dots: From synthesis to photocatalytic applications. Catalysts. 2023;13(4):765. https://doi.org/10.3390/catal13040765

17. Yu J, Wang Y, Huang Y, Wang X, Guo J, Yang J. Structural and electronic properties of SnO_2 doped with non-metal elements. Beilstein J Nanotechnol. 2020;11.1321–1328. https://doi.org/10.3762/bjnano.11.116

18. Akhter P, Arshad A, Saleem A, Hussain M. Recent development in non-metal-doped titanium dioxide photocatalysts for different dyes degradation and the study of their strategic factors: A review. Catalysts. 2022;12(11):1331. https://doi.org/10.3390/catal12111331

19. Gui X, Lu Y, Wang Q, Cai M, Sun S. Application of Quantum Dots for Photocatalytic Hydrogen Evolution Reaction. Appl Sci. 2024;14(12):5333. https://doi.org/10.3390/app14125333

20. Jung H, Sapner VS, Adhikari A, Sathe BR, Patel R. Recent progress on carbon quantum dots based photocatalysis. Front Chem. 2022;10(1):881495. https://doi.org/10.3389/fchem.2022.881495

21. Salunkhe TT, Gurugubelli TR, Babu B, Yoo K. Recent Innovative Progress of Metal Oxide Quantum-Dot-Integrated g-C_3N_4 (0D-2D) Synergistic Nanocomposites for Photocatalytic Applications. Catalysts. 2023;13(11):1414. https://doi.org/10.3390/catal13111414

22. Asahi R, Morikawa T, Ohwaki T, Aoki K, Taga Y. Visible-light photocatalysis in nitrogen-doped titanium oxides. Science. 2001;293(5528):269–271. https://doi.org/10.1126/science.1061051

23. Li D, Huang J, Li R, Chen P, Chen D, Cai M, et al. Synthesis of a carbon dots modified g-C_3N_4/SnO_2 Z-scheme photocatalyst with superior photocatalytic activity for PPCPs degradation under visible light irradiation. J Hazard Mater. 2021;401(1):123257. https://doi.org/10.1016/j.jhazmat.2020.123257

24. Chen YW, Jiang YF, Chen BY, Ye FL, Duan HQ, Cui HY. Facile fabrication of N-doped carbon quantum dots modified SnO_2 composites for improved visible light photocatalytic activity. Vacuum. 2021;191(1):110371. https://doi.org/10.1016/j.vacuum.2021.110371

25. Bubel S, Chabinyc ML. Model for determination of mid-gap states in amorphous metal oxides from thin film transistors. J Appl Phys. 2013;113(23). https://doi.org/10.1063/1.4808457

26. Liu D, Zhao C, Chen M, Yang Y, Qian J, Xie X, et al. Enhanced visible light photocatalytic performance of carbon and oxygen co-doped carbon nitride with a three-dimensional structure: Performance and mechanism study. J Colloid Interface Sci. 2024;665.452–464. https://doi.org/10.1016/j.jcis.2024.03.140

27. Ma H, Teng K, Fu Y, Song Y, Wang Y, Dong X. Synthesis of visible-light responsive Sn-SnO_2/C photocatalyst by simple carbothermal reduction. Energy Environ Sci. 2011;4(8):3067–3074. https://doi.org/10.1039/C1EE01095F

28. Tirado-Guízar A, Pina-Luis GE, Paraguay-Delgado F. Ecofriendly synthesis of ultra-small metal-doped SnO_2 quantum dots. MRS Communications. 2015;5(1):63–69. https://doi.org/10.1557/mrc.2015.11

29. Tsuzuki T, He R, Dodd A, Saunders M. Challenges in determining the location of dopants, to study the influence of metal doping on the photocatalytic activities of ZnO nanopowders. Nanomaterials. 2019;9(3):481. https://doi.org/10.3390/nano9030481

30. Tomer VK, Malik R, Duhan S, Nehra SP, Rana PS. One-pot hydrothermal synthesis of porous SnO_2 nanostructures for photocatalytic degradation of organic pollutants. Energy and Environment Focus. 2015;4(4):340–345. https://doi.org/10.1166/eef.2015.1182

31. Nouri A, Fakhri A. Synthesis, characterization and photocatalytic applications of N-, S-, and C-doped SnO_2 nanoparticles under ultraviolet (UV) light illumination. Spectrochim Acta A Mol Biomol Spectrosc. 2015 Mar 5;138:563-8. https://doi.org/10.1016/j.saa.2014.11.075

32. Reddy GT, Kadam AN, Lee SW, Byon C, Shim J. Enhancement of visible-light-driven photoresponse of Mn-doped SnO_2 quantum dots obtained by rapid and energy efficient synthesis. Journal of Luminescence. 2018;195.283–289. https://doi.org/10.1016/j.jlumin.2017.11.040

33. Ahmed F, Arshi N, Anwar MS, Danish R, Koo BH. Quantum-confinement induced enhancement in photocatalytic properties of iron oxide nanoparticles prepared by ionic liquid. Ceramics International.

2014;40(10):15743–15751. https://doi.org/10.1016/j.ceramint.2014.07.098

34. Wang C, Thompson RL, Ohodnicki P, Baltrus J, Matranga C. Size-dependent photocatalytic reduction of CO_2 with PbS quantum dot sensitized TiO_2 heterostructured photocatalysts. Journal of Materials Chemistry. 2011;21(35):13452–13457. https://doi.org/10.1039/C1JM12367J

35. Babu B, Reddy IN, Yoo K, Kim D, Shim J. Bandgap tuning and XPS study of SnO_2 quantum dots. Materials Letters. 2018;221:211-215. https://doi.org/10.1016/j.matlet.2018.03.107

36. Herrmann JM. Heterogeneous photocatalysis: fundamentals and applications to the removal of various types of aqueous pollutants. Catalysis Today. 1999;53.115–129. https://doi.org/10.1016/S0920-5861(99)00107-8